J. Electrochem. Sci. Eng. **16** (2026) 3177; https://doi.org/10.5599/jese.3177

Open Access : : ISSN 1847-9286
https://pub.iapchem.org/ojs/index.php/JESE

Original scientific paper

Photocatalytic, electrochemical and photoelectrocatalytic degradation of the reactive dye Turquoise Tiafix R2G using $LaFeO_3$ perovskite

Jonh Y. E. Santos[1,✉], Rebeca E. S. Barros[2,3], Katlin I. B. Eguiluz[2,3], Patrícia M. Pimentel[4], Rosane M. P. B. Oliveira[1] and Giancarlo R. Salazar-Banda[2,3]

[1]*Graduate Program in Materials Science and Engineering, Federal University of Sergipe, São Cristovão 49107-230, SE, Brazil*
[2]*Electrochemistry and Nanotechnology Laboratory, Institute of Technology and Research (ITP), Aracaju, SE, Brazil*
[3]*Graduate Program in Process Engineering (PEP), Tiradentes University, Aracaju 49010-390, SE, Brazil*
[4]*Graduate Program in Materials Science and Engineering, Federal Rural University of the Semiarid Region, Mossoró 59625-900, RN, Brazil*

Corresponding Authors: ✉*jonhyago@academico.ufs.br; Tel.: +55-79-3218-2190*

Received: December 19, 2025; Accepted: May 7, 2026; Published: May 12, 2026

Abstract

In this study, the photocatalytic, electrochemical and photoelectrocatalytic performance of lanthanum ferrite ($LaFeO_3$) toward the degradation of the dye Turquoise Tiafix R2G was investigated. $LaFeO_3$ was synthesized via a sol-gel route and characterized by XRD, N_2 adsorption (BET) and SEM, confirming its perovskite structure. Photolysis experiments indicated that the dye is highly photostable under the irradiation conditions employed. In photocatalysis, different $LaFeO_3$ loadings (0.1, 0.2 and 0.3 g L^{-1}) were tested under a 100 W halogen lamp, with 0.3 g L^{-1} providing the highest removal, although the process remained limited by electron-hole recombination. In heterogeneous electro-oxidation with $LaFeO_3$ in suspension, current densities of 10, 15 and 20 mA cm^{-2} were applied; 15 mA cm^{-2} afforded the best compromise between activity and stability, significantly increasing the dye oxidation rate. The simultaneous application of irradiation and current in the photoelectrocatalytic process led to the highest efficiency, achieving approximately 95% degradation within 60 min. These results demonstrate a clear synergistic effect between photocatalytic reactive oxygen species generation in the $LaFeO_3$ suspension and electrochemical oxidant generation at the anode, resulting in a more effective oxidative environment. Thus, the optimized photoelectrocatalytic condition (0.3 g L^{-1} $LaFeO_3$ and 15 mA cm^{-2}) is a promising strategy for the treatment of effluents containing industrial dyes.

Keywords

Dye removal; lanthanum ferrite; photocatalysis; photoelectrocatalysis; degradation kinetics

The intensification of industrial activity, especially in the textile and chemical sectors, has increased the discharge of complex and persistent organic compounds, including reactive dyes, into aquatic environments [1]. Among these contaminants, the reactive dye Turquoise Tiafix R2G is widely employed in dyeing processes and has been recurrently detected in industrial effluents [2].

Even at low concentrations, these dyes pose a major environmental challenge because their highly stable molecular structures, often comprising azo linkages and extended aromatic systems, hinder biodegradation [3]. In this context, the search for advanced and more sustainable dye degradation technologies has stimulated the development of increasingly efficient catalytic materials. Perovskite-type ferrites, such as lanthanum ferrite ($LaFeO_3$), have attracted growing interest owing to their elemental abundance, structural stability and electronic properties that favour light- and/or current-assisted oxidative processes [4].

$LaFeO_3$ has been widely investigated as a photocatalyst and exhibits promising activity toward the degradation of model dyes such as methylene blue [5] and rhodamine B [6]. Recent studies indicate that coupling electro-oxidation with photo-assisted processes can improve dye degradation by combining photocatalytic reactive oxygen species generation (hydroxyl radicals ($^{\bullet}OH$), superoxide ($O_2^{\bullet-}$) and hydrogen peroxide (H_2O_2)) with electrochemically generated oxidants, depending on the reactor configuration [7].

When the semiconductor is dispersed in suspension rather than deposited as a film electrically connected to the circuit, it becomes essential to distinguish between (i) electro-oxidation, which occurs predominantly at the electrode-solution interface, and (ii) the heterogeneous catalytic contribution of the suspended solid, which can act as a redox mediator and participate in chemical steps within the solution volume [8]. Thus, direct comparisons between photocatalysis, electro-oxidation and hybrid operating modes under a common experimental configuration are, therefore, particularly valuable for elucidating the origin of any observed synergies and for employing more precise terminology when describing the role of $LaFeO_3$ in photo-assisted electrochemical systems. Nevertheless, studies that systematically compare the photocatalytic, heterogeneous electro-oxidation and photoelectrocatalytic performance of $LaFeO_3$ under strictly identical conditions remain scarce.

Therefore, exploring the synergy between electro-oxidation in the presence of $LaFeO_3$ in suspension (hereinafter referred to as heterogeneous electro-oxidation) and photoelectrocatalysis using pure ferrites, such as $LaFeO_3$, represents not only an innovative approach to wastewater treatment but also an opportunity to address a relevant gap in the literature. In most reports, $LaFeO_3$ is evaluated separately in either photocatalytic or electrocatalytic mode, and there are still few direct comparative studies, conducted under strictly identical conditions, that can clarify whether the hybrid mode offers energetic and/or mechanistic advantages. Such a comparative strategy contributes to a deeper understanding of the reaction pathways and to a more rigorous assessment of the efficiency and technological applicability of these processes.

Thus, in this work, we synthesized $LaFeO_3$ by a sol-gel route and evaluated its performance toward the degradation of the reactive dye Turquoise Tiafix R2G in aqueous solution by photocatalysis, heterogeneous electro-oxidation and photoelectrocatalysis. The material was characterized by X-ray diffraction (XRD), N_2 adsorption-desorption (Brunauer-Emmett-Teller (BET) surface area) and scanning electron microscopy (SEM). Dye degradation was monitored by UV-Vis spectrophotometry with the aim of correlating the structural and textural properties of $LaFeO_3$ with the performance and kinetics of the three processes.

Experimental

Reagents

The reactive dye Turquoise Tiafix R2G, supplied by Aupicor Química Ltda. (Brazil), was used as the model pollutant in all degradation experiments. According to the manufacturer's safety data sheet, this product is a vinyl sulfone-type reactive phthalocyanine dye. Commercial turquoise reactive phthalocyanine dyes of this type are commonly associated with C.I. Reactive Blue 21 (RB21), a copper phthalocyanine reactive dye used in textile applications. RB21 is reported with CAS No. 12236-86-1, molecular formula $C_{40}H_{25}CuN_9O_{14}S_5$, and molecular weight of approximately 1079.6 to 1080 g·mol^{-1}; reported synonyms include Reactive Blue 21, C.I. Reactive Blue 21, Turquoise Blue G-133 and Sumifix Turquoise Blue G [9,10].

Because Turquoise Tiafix R2G is a commercial formulated dye rather than a purified analytical standard, it may contain structurally related dye species, salts, synthesis by-products and other formulation components. Therefore, a unique chemical structure, exact molecular formula, or exact molar mass cannot be assigned specifically to the commercial product. The manufacturer does not report a nominal purity percentage. Accordingly, the dye was used as received, without additional purification, and the concentrations reported in this work refer to the mass concentration of the commercial dye product. A stock solution was prepared by dissolving Turquoise Tiafix R2G in deionized water to obtain a concentration of 200 mg L^{-1}, from which all working solutions were prepared.

The supporting electrolyte consisted of 0.1 mol·L^{-1} of Na_2SO_4 and 100 ppm of NaCl, prepared in 100 mL of ultrapure water (Gehaka MS 2000 purification system). Na_2SO_4 was selected because sulphate is relatively stable under the applied conditions and is commonly used as a supporting electrolyte in electrochemical advanced oxidation processes, where it generally has limited direct interaction with organic pollutants [11]. NaCl was added at 100 ppm to simulate the presence of chloride commonly found in textile effluents and to promote limited in situ formation of active chlorine species, including Cl_2, HOCl and ClO^-, which may contribute to oxidative dye degradation, thereby enhancing the overall degradation efficiency [12]. The experiments were conducted at pH 6 and at 300 K.

Synthesis of the $LaFeO_3$ catalyst

$LaFeO_3$ powder was synthesized by a modified sol-gel route using $La(NO_3)_3{\cdot}6H_2O$ (99 %, Sigma Aldrich) and $Fe(NO_3)_3{\cdot}9H_2O$ (99 %, Sigma Aldrich) in a 1:1 molar ratio (La:Fe). Initially, gelatine was placed in a beaker and dissolved in 150 mL of deionized water under constant stirring at 50 °C. The metallic nitrates were then added, and the mixture was homogenized for 1 h at 70 °C. Subsequently, the temperature was increased to approximately 90 °C and maintained under stirring until the formation of a viscous gel. The resulting gel was first calcined at 400 °C for 2 h, using a heating rate of 10 °C min^{-1}, to decompose the organic precursors. The obtained powders were then calcined at 1000 °C for 4 h, at a heating rate of 10 °C min^{-1}, to promote the formation of the $LaFeO_3$ perovskite phase.

Physical characterization

The crystalline structure of the calcined $LaFeO_3$ powder was analysed by X-ray diffraction (XRD) using a Shimadzu XRD-7000 diffractometer equipped with a Cu anode (Kα = 0.15418 nm). Diffractograms were collected over the 2θ range of 20 to 80° with a scanning rate of 0.02° min^{-1}. The morphology was analysed by scanning electron microscopy (SEM) using TESCAN VEGA's 4th generation microscope. The specific surface area was determined by BET method from nitrogen adsorption-desorption isotherms measured on a NOVA 1000e surface area & pore size analyser (Quantachrome). Before the measurements, all samples were degassed at 150 °C for 3 h. The specific surface area (SBET)

was calculated from the adsorption branch of the N_2 adsorption-desorption isotherm using BET equation within the relative pressure range in which the BET plot was linear. The mesopore size distribution and mesopore volume were determined from the desorption branch using the Barrett-Joyner-Halenda (BJH) method with the Harkins-Jura thickness model, following standard procedures for mesoporous materials [13]. In addition, the pore size distribution was also evaluated by density functional theory (DFT), applying a nitrogen adsorption kernel suitable for micro- and mesoporous materials at 77 K [14]. All BET, BJH and DFT calculations were performed using the instrument's proprietary analysis software.

Degradation of Turquoise Tiafix R2G

The photolysis experiments were first carried out to evaluate the stability of the dye in the absence of a catalyst and to verify whether the applied radiation could promote direct photodegradation. An aliquot of 100 mL of the aqueous Turquoise Tiafix R2G solution was kept under magnetic stirring in the dark for 30 min at 27 °C to ensure system equilibration.

The solution was then irradiated with a 100 W halogen lamp, with an irradiance of 2.87 W cm^{-2} at the solution surface, which served as the light source for the photolytic process. Throughout the experiment, 2 mL aliquots were withdrawn at 0, 2, 5, 10, 15, 30 and 60 min and analysed using a Shimadzu UV-Vis spectrophotometer (UV-1900i).

For the photocatalytic evaluation of $LaFeO_3$, suspensions were prepared at different catalyst loadings (0.1, 0.2 and 0.3 g L^{-1}) in 100 mL of the aqueous Turquoise Tiafix R2G solution. The suspensions were magnetically stirred in the dark for 30 min at 27 °C to achieve good dispersion and adsorption equilibrium. Subsequently, the suspensions were irradiated with the same halogen lamp used in the photolysis experiments. During irradiation, 2 mL aliquots were collected at 0, 2, 5, 10, 15, 30 and 60 min and analysed by UV-Vis spectrophotometry.

Electrochemical and photoelectrocatalytic oxidations were performed in a single-compartment electrochemical cell with an interelectrode distance of 1.0 cm and a useful volume of 150 mL. The electrochemical system employed a $Ti/(RuO_2)_{0.8}$-$(Sb_2O_4)_{0.2}$ anode with a geometric area of 2 cm^2, prepared *via* the Pechini method and calcined at 350 °C using a CO_2 laser protocol, as previously reported [15]. A platinum plate with the same geometric area (2 cm^2) was used as the counter electrode. Prior to each experiment, the electrolyte solution was continuously purged with N_2 to remove residual dissolved oxygen.

Galvanostatic electrolyses were carried out at current densities of 10, 15 and 20 mA cm^{-2} using a FA-3005-M current source. In the photoelectrocatalytic assays, suspensions containing $LaFeO_3$ were irradiated under the same conditions as in the photocatalytic tests while the current was applied.

The photodegradation, electrodegradation and photoelectrodegradation of Turquoise Tiafix R2G were monitored by measuring the absorbance at the characteristic band near 620 nm using a UV-Vis spectrophotometer over the 600-700 nm range. The calibration curve was constructed from a 200 ppm stock solution of the dye, suitably diluted to obtain concentrations of 5, 10, 25, 50, 75, 100, 150 and 200 ppm, and used to determine the dye concentration in the aliquots collected at the specified times. The degradation kinetics of R2G were subsequently evaluated from the temporal concentration profiles.

High-performance liquid chromatography (HPLC) analyses were performed to further evaluate dye degradation using samples collected under the best-performing condition (photoelectrocatalysis at 15 mA cm^{-2}). The analyses were carried out using a reverse-phase HPLC system equipped with a photodiode array detector.

Chromatographic separation was performed on a C18 column (150×2.1 mm, 3 µm particle size). The mobile phase consisted of aqueous ammonium formate (NH_4HCO_2) solution (20 mM, pH 6.4) as solvent A and acetonitrile (CH_3CN) containing 0.1 % formic acid (HCOOH) as solvent B. Gradient elution was applied at a flow rate of 0.2 mL min^{-1} and a column temperature of 20 °C, starting at 1 % B, increasing to 99 % B, and then returning to initial conditions. The injection volume was 4 µL. Before analysis, the samples were filtered through 0.22 µm membrane filters to remove suspended catalyst particles. Detection was carried out at 620 nm, corresponding to the maximum absorption wavelength of the dye.

Quantification of the dye signal was performed using an external calibration curve prepared over the concentration range of 5 to 200 ppm. Linear regression of peak area versus concentration was used to estimate the concentration of the dye. Samples collected during the photoelectrocatalytic treatment from 0 to 60 min were analysed under identical chromatographic conditions. Dye degradation was evaluated from the decrease in the main chromatographic peak assigned to the dye, together with the appearance and evolution of additional peaks associated with transformation products.

The stability and reusability of the catalyst were evaluated under photocatalytic conditions through consecutive degradation cycles using the optimized parameters. After each reaction cycle, the catalyst was recovered by decantation and dried under ambient conditions. The recovered catalyst was then reused directly in the next photocatalytic cycle under the same experimental conditions. This procedure was repeated for four consecutive cycles. The degradation performance was monitored by UV-Vis spectrophotometry by following the normalized concentration, C/C_0 (C and C_0 are the dye concentrations at time t and at the beginning of the experiment, respectively) and the degradation efficiency, %, at the maximum absorption wavelength of the dye, 620 nm.

Results and discussion

Structural and morphological aspects of $LaFeO_3$

To confirm the formation of the desired crystalline phase and assess the efficiency of the synthesis procedure, the X-ray diffraction (XRD) pattern of the calcined $LaFeO_3$ powder was recorded (Figure 1).

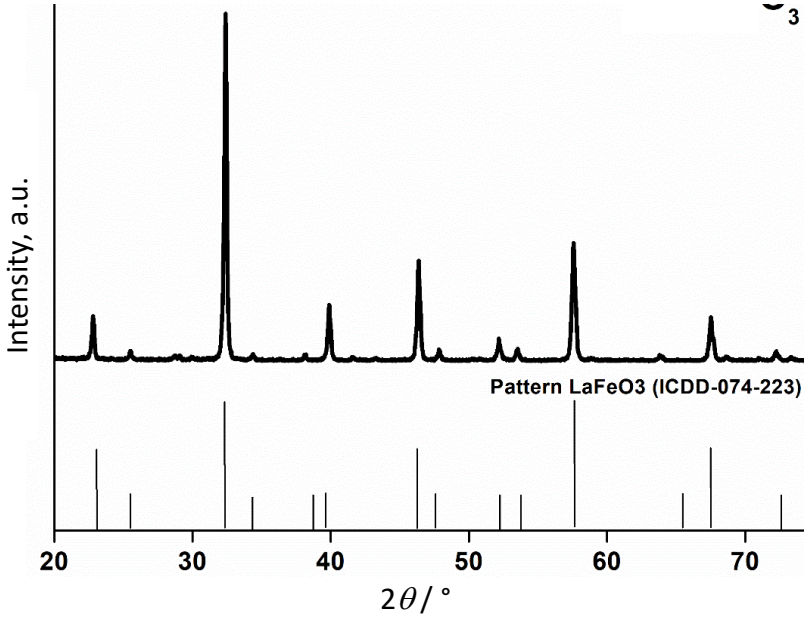

Figure 1. *X-ray diffraction pattern of $LaFeO_3$ synthesized by the sol-gel method and calcined at 1000 °C*

The diffraction pattern exhibits all characteristic reflections of orthorhombic $LaFeO_3$ perovskite, in agreement with the ICDD reference pattern 00-074-2203. The main peaks at 2θ = 22.65, 32.25, 39.77, 46.25 and 57.50° can be indexed to the (101), (121), (220), (202) and (240) planes, respectively, confirming the formation of the targeted crystal structure. Additional reflections of lower intensity at 52.09 and 67.48° are also consistent with the orthorhombic arrangement.

The consistent set of reflections associated with orthorhombic $LaFeO_3$ indicates high phase purity, since no diffraction peaks attributable to residual Fe_2O_3 or La_2O_3 were detected within the sensitivity limits of the measurements [16].

The sharp and intense peak centred at 32.25° suggests a high degree of crystallinity and relatively well-developed crystallites. This behaviour is typical of $LaFeO_3$ samples subjected to elevated calcination temperatures that promote pronounced crystal growth [17]. The textural properties of $LaFeO_3$ were evaluated from N_2 adsorption-desorption isotherms using the BET method. Table 1 summarizes the BET, BJH (Barrett-Joyner-Halenda) and DFT (Density Functional Theory) surface areas, as well as the total pore volume and average pore radius. The BJH and DFT pore area values reported in Table 1 correspond to the cumulative pore surface areas calculated by the instrument software from the respective pore size distribution models.

Table 1. *Textural properties of $LaFeO_3$ obtained from N_2 adsorption-desorption isotherms*

BET area, $m^2\ g^{-1}$	BJH area, $m^2\ g^{-1}$	DFT area, $m^2\ g^{-1}$	Pore volume, $cm^3\ g^{-1}$	Pore radius, nm
0.674	1.908	2.415	0.005	1.911

The BET specific surface area was 0.674 $m^2\ g^{-1}$, indicating that the material has a low specific area. This behaviour is expected for perovskites calcined at high temperatures, for which extensive crystal growth and sintering lead to coarsened particles and a marked reduction in surface area [18]. Such features have been widely reported for lanthanum orthoferrites synthesized under similar conditions [17,18].

The surface areas estimated from BJH (1.908 $m^2\ g^{-1}$) and DFT (2.415 $m^2\ g^{-1}$) analyses, although slightly higher than the BET value, remain low and indicate only a small contribution from accessible pores resolved by pore-size distribution methods. These results confirm that the material does not exhibit a well-developed mesoporous texture, but instead has a predominantly dense, weakly porous structure, in line with the high crystallinity observed by XRD [17,19].

The total pore volume found (5 $mm^3\ g^{-1}$) confirms the low porosity of the material, indicating that the pores present are scarce and have a small internal volume. The average pore calculated radius (~1.9 nm (19 Å)) lies near the boundary between micropores and the onset of the mesopore range. This suggests the presence of narrow pores, likely formed by gas release during the decomposition of organic precursors, without the development of an extended, interconnected porous network. Overall, the XRD and textural data indicate that the $LaFeO_3$ obtained by the sol-gel route followed by high-temperature calcination is a highly crystalline lanthanum ferrite with low specific surface area and limited porosity, as typically reported for well-crystallized $LaFeO_3$ perovskites [17,18,20].

Morphological characterization was performed by SEM to evaluate particle distribution, degree of agglomeration and surface characteristics of $LaFeO_3$. Figure 2 shows micrographs obtained at different magnifications.

The SEM images reveal that $LaFeO_3$ consists of particles with irregular morphology, strongly agglomerated and lacking clearly defined individual contours. This behaviour is typical of perovskite-type oxides synthesized by chemical routes involving organic precursors [21]. The presence of these compact agglomerates is directly associated with the calcination process, which promotes partial

sintering and coalescence of the particles, resulting in dense and poorly porous structures [22]. This observation is consistent with the high crystallinity evidenced by XRD and the low surface area determined by BET.

The morphology observed by SEM is in line with the XRD results, which confirmed the formation of a single, highly crystalline phase corresponding to orthorhombic $LaFeO_3$. The narrow and well-defined diffraction peaks, matching the ICDD 00-074-2203 reference pattern, indicate a high degree of crystallinity and pronounced crystallite growth. Such crystal growth typically reduces the available surface area by increasing the average particle size, thus favouring sintering and agglomeration, as observed in the SEM micrographs.

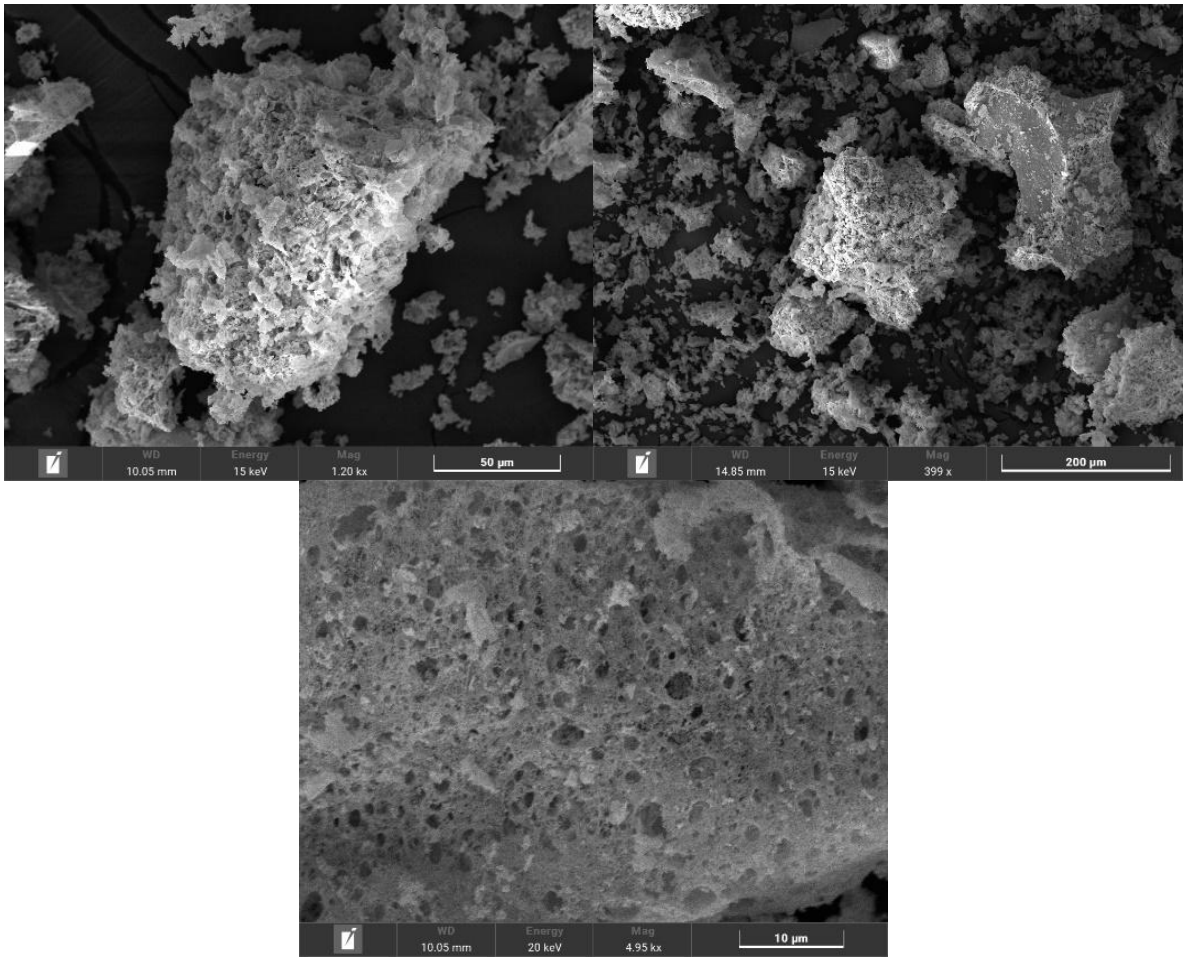

Figure 2. *SEM micrographs of $LaFeO_3$ at different magnifications*

Textural analysis (BET, BJH and DFT) complements these results by revealing that the sample has a low specific surface area (0.674 $m^2\ g^{-1}$), a small total pore volume (5 $mm^3\ g^{-1}$) and an average pore radius of ~1.9 nm. This pore radius lies near the boundary between micropores and the onset of the mesoporous range and reflects the presence of narrow pores rather than a well-developed, interconnected porous network. These parameters confirm that the material has limited internal accessibility, consistent with the dense agglomerates observed by SEM and the high crystallinity revealed by XRD.

In general, the morphology observed by SEM, characterized by agglomerated particles with compact surfaces, is coherent with the high crystallinity determined by XRD and the low surface area measured by BET. Although the reduced specific surface area implies limited external surface availability, this feature does not necessarily preclude the catalytic use of $LaFeO_3$. In such perovskite oxides, catalytic activity is not governed solely by dye adsorption but is strongly influenced by

intrinsic electronic and redox properties [23,24]. The Fe^{3+}/Fe^{2+} alternation capacity [25], the oxygen mobility in the lattice, and the ability to generate reactive oxygen species are key factors that can sustain significant catalytic performance even in low-porosity materials [26]. Thus, the structural, morphological, and textural characteristics obtained for $LaFeO_3$ support its further evaluation as a catalyst for the degradation of the reactive dye Turquoise Tiafix R2G.

Evaluation of catalytic activity in R2G degradation

After confirming the structural and textural properties of $LaFeO_3$, its performance in the degradation of the industrial dye Turquoise Tiafix R2G (hereafter denoted R2G) was evaluated. Catalytic experiments were conducted using three complementary approaches: photocatalysis, heterogeneous electro-oxidation and photoelectrocatalysis, seeking to understand how catalyst loading and applied current influence the efficiency and kinetics of the oxidative process.

Initially, the effect of catalyst loading on dye photodegradation was evaluated. Photocatalytic tests were performed using 0.1, 0.2 and 0.3 g L^{-1} of $LaFeO_3$ in 100 mL of a 200 ppm aqueous R2G solution. Before the degradation experiments, the dye solution or dye-catalyst suspension was magnetically stirred in the dark for 30 min at 27 °C to ensure proper dispersion and establish adsorption-desorption equilibrium, as commonly reported for heterogeneous photocatalytic systems. To show this pre-reaction stage in the kinetic profiles, negative time values, -30, -20 and -10 min, were used in Figures 3 to 5. These points correspond only to the dark equilibration period, during which irradiation and/or current application had not yet started. The reaction time was defined as t = 0 min, corresponding to the onset of irradiation and/or current application. This procedure allows the contribution of initial adsorption to be distinguished from the degradation stage and prevents overestimation of the treatment efficiency [27]. The suspension was then irradiated with a 100 W lamp. In parallel, photolysis experiments were performed in the absence of the catalyst.

Figure 3 shows the evolution of the normalized concentration (C/C_0) during the photodegradation of Turquoise Tiafix R2G under different $LaFeO_3$ loadings. The inset plot illustrates the corresponding degradation efficiency, %, allowing direct comparison of the photocatalytic performance under each condition.

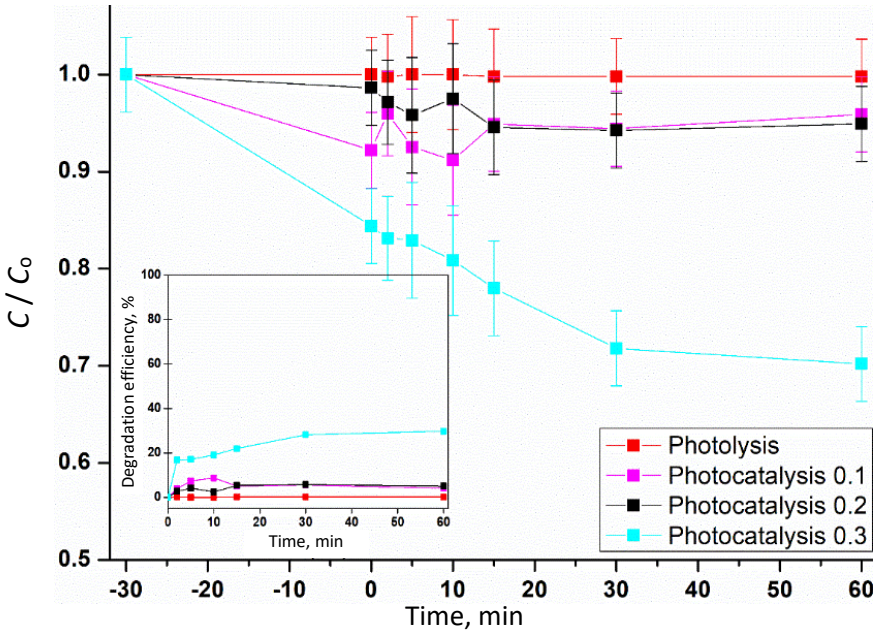

Figure 3. *Photolysis and photocatalytic degradation of Turquoise Tiafix R2G dye (200 ppm) as a function of treatment time under different $LaFeO_3$ loadings (0.1, 0.2 and 0.3 g L^{-1}). Inset: degradation efficiency as a function of time*

In the photolysis control, C/C_0 remained close to unity throughout the experiment, indicating that irradiation with the 100 W lamp in the absence of $LaFeO_3$ was not sufficient to promote significant dye degradation. This behaviour is consistent with several reports showing that isolated photolysis is generally ineffective for industrial dyes, owing to their highly stable molecular structures and low susceptibility to direct photon-induced oxidation [28,29]. In similar systems, degradation by photolysis rarely exceeds 5 to 10 % even under intense UV-Vis irradiation, which reinforces the need for a semiconductor catalyst to initiate and sustain the oxidative process [30].

Several studies have confirmed that direct photolysis of industrial dyes, carried out without catalysts or other advanced oxidation processes, typically leads to limited colour removal [29]. This is attributed to the presence of robust chromophoric groups and conjugated structures that confer high photostability. For instance, in the case of methylene blue, less than 8 % degradation has been reported after 10 h of photolysis, and virtually no decomposition occurs under visible light in the absence of a catalyst [28].

The samples containing 0.1 and 0.2 g L^{-1} of $LaFeO_3$ showed similar C/C_0 profiles, with only modest decreases in dye concentration and stabilization near $C/C_0 \approx 0.90$, corresponding to approximately 10 % degradation of R2G. These results suggest that, at these catalyst loadings, the density of accessible active sites and the extent of photon capture are insufficient to sustain the continuous generation of electron-hole (e^-/h^+) pairs required for effective formation of oxidizing species ($^{\bullet}OH$, $O_2^{\bullet-}$) [31] reported similar behaviour for TiO_2/XG systems, in which low catalyst loadings led to slower degradation kinetics due to the reduced number of active sites and limited photon interception.

Studies involving other perovskites, such as $LaCoO_3$ and $LaMnO_3$, corroborate this behaviour and show that photocatalytic efficiency increases only when the catalyst loading exceeds a minimum threshold required to ensure sufficient optical absorption and surface exposure [32].

On the other hand, at a loading of 0.3 g L^{-1}, $LaFeO_3$ exhibited the best photocatalytic performance, reaching approximately 30 % degradation of R2G. This marked improvement relative to lower loadings can be attributed to more efficient generation of reactive oxygen species, such as $^{\bullet}OH$ and $O_2^{\bullet-}$, upon photoactivation of the perovskite. Under irradiation, electron excitation from the valence band to the conduction band produces e^-/h^+ pairs. Conduction-band electrons can be captured by dissolved oxygen to form $O_2^{\bullet-}$, whereas valence-band holes oxidize water or surface hydroxyl groups, leading to the formation of $^{\bullet}OH$. Similar photocatalytic mechanisms have been reported for other perovskite oxides [17,33].

After identifying 0.3 g L^{-1} $LaFeO_3$ as the most effective photocatalyst loading, the influence of applied current density (10, 15 and 20 mA cm^{-2}) on the electrochemical degradation process was evaluated to investigate the possible synergy between external current application and perovskite activity. Figure 4 shows the evolution of the C/C_0 ratio as a function of electrolysis time for different current densities. The inset presents the corresponding degradation efficiency.

At 10 mA cm^{-2}, a gradual decrease in concentration was observed, reaching 53 % degradation. Although this condition is effective, the relatively modest removal suggests a lower rate of electrogenerated oxidant formation and slower acceleration of the Fe^{3+}/Fe^{2+} redox cycle. Studies on electroactivated perovskites indicate that low current densities favour slower electron-transfer processes, thereby limiting the overall degradation process [34]. In such systems, the efficiency of charge transfer strongly depends on the applied potential and current: at low currents, the limited flow of charge carriers restricts the generation of oxidative species required for dye degradation [7,35].

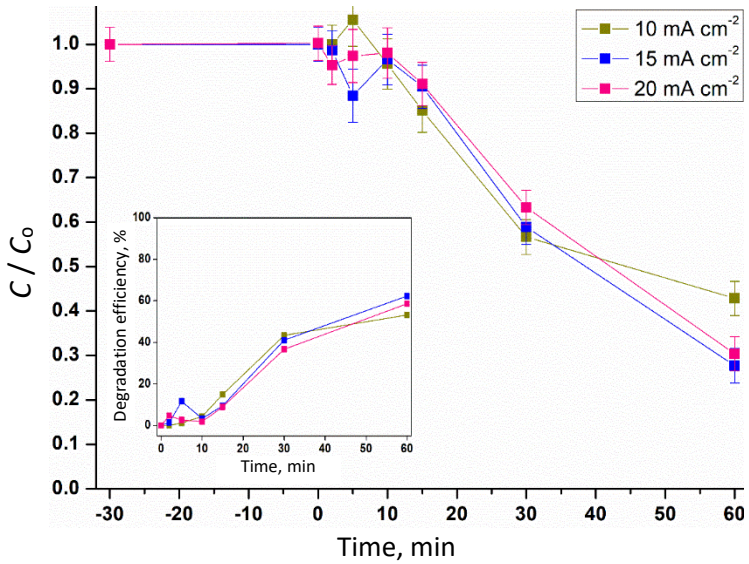

Figure 4. *Electrochemical degradation of Turquoise Tiafix R2G dye (200 ppm) as a function of treatment time at different current densities. Inset: the corresponding degradation efficiency*

The application of 15 mA cm^{-2} resulted in the highest degradation efficiency among the evaluated current densities, with 62 % degradation after 60 min. This behaviour can be attributed to an increased rate of electrogenerated oxidant formation and enhanced charge transport through the perovskite-containing system. Studies on $LaBO_3$-type perovskites in electrocatalytic applications have shown that intermediate current densities often yield optimal performance, as they balance efficient oxidant production with controlled surface conditions, avoiding excessive surface passivation, electrochemical corrosion and unproductive charge recombination [36].

When the current density was increased to 20 mA cm^{-2}, the degradation efficiency decreased slightly (58 % degradation). This decline can be associated with the higher overpotentials required at elevated currents, which favour competitive reactions such as the oxygen evolution reaction (OER) and may lead to surface saturation or blockage of active sites. Under these conditions, a larger fraction of the applied current is diverted to side reactions, reducing the fraction available for target pollutant oxidation.

The literature indicates that beyond a certain limit, further increases in current density no longer translate into more useful radical generation but instead result in higher energy consumption and intensified parasitic reactions. High current densities can promote mass-transport limitations, accumulation of undesired by-products and reduced current efficiency due to the prevalence of parallel reactions [37,38].

Given that photocatalysis with 0.3 g L^{-1} $LaFeO_3$ achieved only moderate degradation, and that electrochemical oxidation alone did not lead to complete removal of R2G, the system was subsequently operated in photoelectrocatalytic mode by combining irradiation with applied current. Figure 5 shows the evolution of C/C_0 as a function of time under simultaneous irradiation and current application. The inset presents the corresponding degradation efficiency.

Under photoelectrocatalytic conditions at 10 mA cm^{-2}, a marked decrease in dye concentration was observed (*i.e*. 60 % degradation of R2G after 60 min). This removal is clearly higher than that obtained under isolated photocatalysis (~30 % degradation) and exceeds the photo-activity observed in the absence of current. It also improves upon the performance at the same current density under purely electrochemical conditions, highlighting the beneficial effect of combining irradiation and applied current.

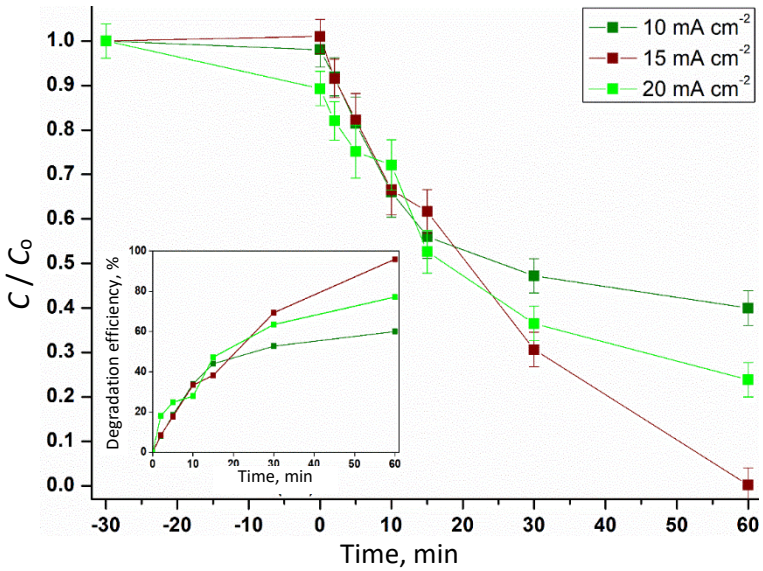

Figure 5. *Photoelectrocatalytic degradation of Turquoise Tiafix R2G dye (200 ppm) as a function of treatment time at different current densities. Inset: the corresponding degradation efficiency*

The photoelectrocatalytic system operated at 15 mA cm^{-2} exhibited the best performance among the evaluated conditions, with C/C_0 decreasing to approximately 0.05 after 60 min, *i.e.* about 95 % dye degradation. This pronounced improvement can be ascribed to a favourable balance between electrochemical driving force and surface stability. Some reports have demonstrated that photoelectrochemical efficiency often reaches a maximum at intermediate current or potential values, whereas excessive currents typically lead to performance losses due to enhanced charge-carrier recombination and electrode or catalyst degradation. The substantial gain in efficiency in the combined current + light mode, approaching 95 % degradation in 60 min under optimized conditions, supports the presence of a synergistic effect. This synergy can be more safely attributed to the simultaneous occurrence of photocatalytic reactive oxygen species generation in the $LaFeO_3$ suspension and electrochemical oxidant generation at the anode, particularly chlorine-based oxidants in the chloride-containing electrolyte, as described in the photoelectrocatalysis literature [39].

Although photoelectrocatalysis at 20 mA cm^{-2} yielded better performance than at 10 mA cm^{-2}, it did not surpass that at 15 mA cm^{-2}. At 20 mA cm^{-2}, C/C_0 reached ≈ 0.22 after 60 min, corresponding to 78 % dye degradation and indicating a decrease in efficiency relative to 15 mA·cm^{-2}. This decline can be associated with the higher overpotentials required at elevated current densities, which enhance the OER, a major competitive pathway that diverts current away from pollutant oxidation [40,41]. In addition, the excess charge-carrier flux at high current densities can promote enhanced charge recombination and the formation of non-productive intermediates, thereby reducing overall current efficiency [42].

Figure 6 compares the best-performing conditions identified for each process: photocatalysis with 0.3 g L^{-1} $LaFeO_3$, heterogeneous electrochemical oxidation at 15 mA cm^{-2} and photoelectrocatalysis at 15 mA cm^{-2}. The inset shows the corresponding degradation efficiency. The purpose of this comparison is to clearly illustrate the progressive enhancement of oxidative performance when transitioning from photocatalysis to heterogeneous electro-oxidation and ultimately to their combination in photoelectrocatalysis.

Photocatalysis with 0.3 g L^{-1} $LaFeO_3$ exhibited moderate performance, achieving around 30 % degradation, likely limited by charge-carrier recombination and the relatively low surface area of the catalyst.

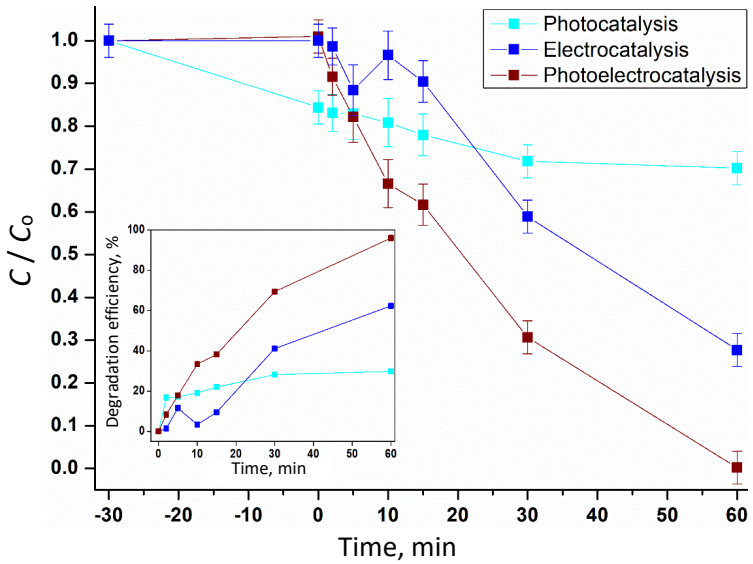

Figure 6. *Comparison of the most efficient conditions for Turquoise Tiafix R2G (200 ppm) degradation: photocatalysis with 0 3 g L^{-1} $LaFeO_3$, heterogeneous electro-oxidation at 15 mA cm^{-2} and photoelectrocatalysis at 15 mA cm^{-2}. Inset: degradation efficiency*

Under heterogeneous electro-oxidation at 15 mA cm^{-2}, dye removal increased significantly to approximately 62 % degradation, demonstrating the positive impact of applying an external current to drive oxidative processes. In contrast, photoelectrocatalysis at 15 mA cm^{-2} led to almost complete degradation of R2G, reaching about 95 % removal within 60 min.

Mechanism of dye degradation

Based on the experimental results and literature reports, a plausible degradation mechanism can be proposed for the photocatalytic, electrochemical and photoelectrocatalytic treatment of Turquoise Tiafix R2G.

Under photocatalytic conditions, irradiation of $LaFeO_3$ with photons of sufficient energy promotes the formation of electron-hole pairs (e^-/h^+) in the semiconductor. The photogenerated holes may oxidize water molecules or hydroxide ions to form hydroxyl radicals (•OH), while the photogenerated electrons may reduce dissolved oxygen to superoxide radicals. Subsequent reactions involving $O_2^{\bullet-}$, HO_2•, H_2O_2 and •OH can generate additional oxidizing species. These reactive oxygen species can attack the phthalocyanine chromophore and other organic moieties of the dye, leading to decolorization and progressive chemical transformation of the pollutant [43,44].

In the electrochemical process, degradation occurs at or near the $Ti/(RuO_2)_{0.8}$-$(Sb_2O_4)_{0.2}$ anode through both direct and indirect oxidation pathways. Direct oxidation may occur by electron transfer from the dye or adsorbed intermediates to the anode surface. Indirect oxidation may occur through oxidants generated electrochemically from water and electrolyte species. In aqueous electrolyte, water oxidation at the anode can produce adsorbed hydroxyl species, whereas in the presence of chloride ions, chlorine-based oxidants such as Cl_2, HOCl and ClO^- may be formed. These species can react with the dye in the solution phase and contribute to the degradation of the chromophoric structure [45-47].

In photoelectrocatalysis, the photocatalytic and electrochemical pathways operate simultaneously. Under light irradiation, suspended $LaFeO_3$ particles promote photocatalytic charge-carrier generation and subsequent formation of reactive oxygen species. At the same time, the $Ti/(RuO_2)_{0.8}$-$(Sb_2O_4)_{0.2}$ anode promotes the formation of electrochemical oxidants, particularly active chlorine species in the chloride-containing electrolyte. Thus, the photoelectrocatalytic process can be

understood as the combination of photocatalytic reactive oxygen species generation in the $LaFeO_3$ suspension and electrochemical oxidant generation at the anode. The coexistence of reactive oxygen species and electrochemically generated oxidants creates a more effective oxidative environment, which explains the higher degradation efficiency observed for the photoelectrocatalytic process compared with photocatalysis or electrochemical oxidation alone [45,47].

The $Ti/(RuO_2)_{0.8}$-$(Sb_2O_4)_{0.2}$ anode is expected to play a key role in electrochemical and photoelectrocatalytic systems. The Ti substrate provides mechanical stability and electrical conductivity, while RuO_2 acts as the main electrocatalytically active oxide phase for water and chloride oxidation. The Sb oxide component may contribute to electrode stability and modify the electrochemical properties of the mixed oxide surface, influencing the formation of oxidizing species and the competition with oxygen evolution [48]. Therefore, in the Na_2SO_4/NaCl electrolyte used in this work, the anode contributes to dye degradation mainly by promoting indirect oxidation through surface hydroxyl species and chlorine-based oxidants [46].

UV-Vis absorption spectra of R2G

To support the degradation results obtained from the C/C_0 profiles and to confirm the wavelength selected for monitoring dye removal, UV-Vis absorption spectra were recorded for Turquoise Tiafix R2G before and after each of the different treatment processes. Figure 7 shows the spectra of the initial dye solution and of the solutions treated by photolysis, photocatalysis, electrochemical oxidation and photoelectrocatalysis.

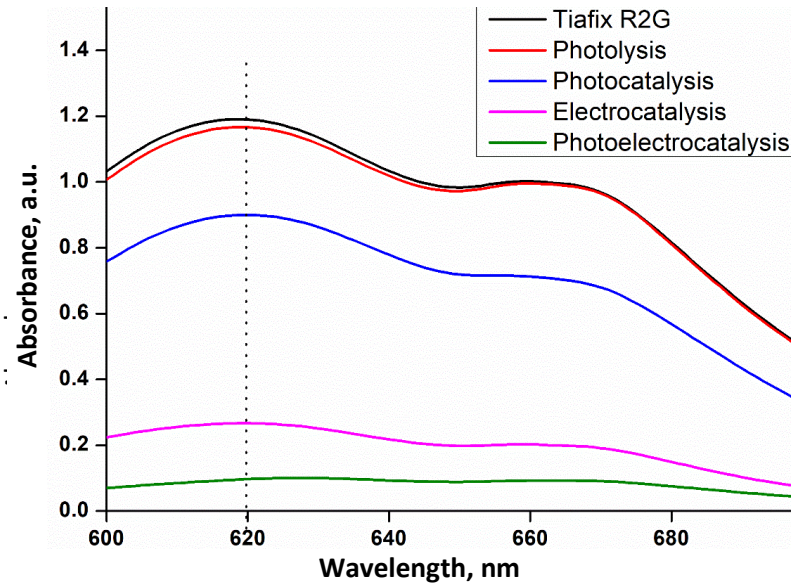

Figure 7. *UV-Vis absorption spectra of Turquoise Tiafix R2G (200 ppm) under different conditions: initial solution and after photolysis, photocatalysis, electrochemical oxidation and photoelectrocatalysis*

As shown in Figure 7, the initial dye solution exhibits a pronounced absorption maximum at approximately 620 nm, which is attributed to the Q band of the phthalocyanine chromophore. The decrease in absorbance at this wavelength after treatments indicates progressive disruption of the chromophoric system, while the absence of significant peak shifts suggests that its fundamental electronic structure is initially preserved. In some cases, a secondary band around ~670 nm is observed, possibly associated with intermediate species formed during the degradation process. Among the evaluated processes, photoelectrocatalysis produced the largest reduction in the 620 nm absorption band, confirming its higher degradation efficiency under the experimental conditions used in this study [49].

Kinetics of R2G degradation

Following this comparative evaluation of the photocatalytic, electrochemical and photoelectrocatalytic systems, a kinetic analysis was performed to quantify the degradation rate under the most efficient conditions, as shown in Figure 8. This figure shows the kinetic curves obtained for the photocatalytic, electrochemical oxidation and photoelectrocatalytic systems, fitted to a pseudo-first-order model. The linear behaviour of $\ln(C/C_0)$ as a function of time indicates that this model adequately describes the dye degradation kinetics under the different operating conditions.

The pseudo-first-order approach is widely applied to photo(electro)catalytic degradation of organic pollutants, as demonstrated in several studies involving $LaFeO_3$, $LaCoO_3$ and $LaMnO_3$ perovskites [17,21,50]. In the present case, the photocatalytic curve exhibits a small slope, with data points clustered near the upper region of the plot ($\ln(C/C_0) \approx 0$ to -0.5), reflecting the modest degradation observed experimentally. The heterogeneous electro-oxidation curve shows an intermediate slope, with $\ln(C/C_0)$ values reaching approximately -1.5 at 60 min, confirming that the electrochemical process significantly accelerates dye removal compared with photocatalysis alone.

In contrast, the photoelectrocatalytic curve displays the steepest slope, with $\ln(C/C_0)$ values dropping below -6 at 60 min, indicative of very fast kinetics. The marked linearity of this curve further supports the suitability of the pseudo-first-order description for the PEC process under the studied conditions.

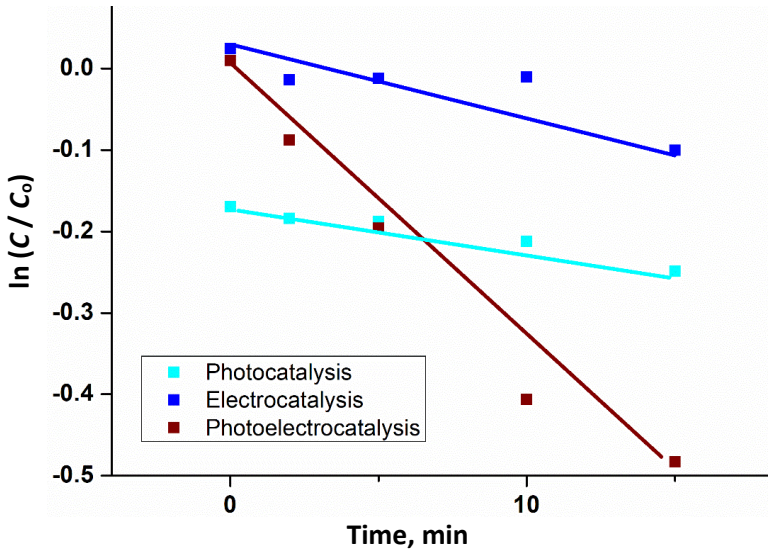

Figure 8. *Pseudo-first-order kinetic plots for the degradation of Turquoise Tiafix R2G (200 ppm) under photocatalysis (0.3 g L^{-1} $LaFeO_3$), heterogeneous electro-oxidation (15 mA cm^{-2}) and photoelectrocatalysis (15 mA cm^{-2})*

The apparent rate constants (k) were obtained from the linear fits using the pseudo-first-order expression, Equation (1):

$$\ln\left(\frac{C}{C_0}\right) = -kt \quad (1)$$

The resulting kinetic parameters are summarized in Table 2.

Photocatalysis with 0.3 g L^{-1} $LaFeO_3$ yielded an apparent rate constant of 0.00595 min^{-1}, confirming that, despite the increased catalyst loading, the process remains kinetically limited. This low k value is consistent with the moderate degradation observed experimentally and is in line with previous reports, which often describe k values below 0.01 min^{-1} for undoped perovskites operating under simple photocatalytic conditions, particularly when targeting structurally complex dyes [51].

Under electrocatalytic conditions at 15 mA cm^{-2}, the apparent rate constant increased to 0.01610 min^{-1}, corresponding to an approximately threefold enhancement relative to photocatalysis. This substantial increase underscores the direct impact of applying an external current on the generation of oxidizing species and the acceleration of degradation reactions.

***Table 2**. Apparent pseudo-first-order kinetic parameters for R2G degradation under different conditions*

Process	ln (C / C_o)	k / min^{-1}	Relative increase in k versus photocatalysis
Photocatalysis (0.3 g L^{-1})	-0.357	0.00595	
Heterogeneous electro-oxidation (15 mA cm^{-2})	-0.967	0.01610	2.7-fold higher than photocatalysis
Photoelectrocatalysis (15 mA cm^{-2})	-2.996	0.04990	8.4-fold higher than photocatalysis 3.1-fold higher than electro-oxidation

The photoelectrocatalytic (PEC) system at 15 mA cm^{-2} exhibited a pronounced kinetic enhancement, with k = 0.04990 min^{-1}, approximately 8 times higher than for photocatalysis and about 3 times higher than for electrocatalysis alone. This high rate constant provides quantitative evidence of a synergistic effect between light irradiation and applied current, confirming that PEC is the fastest and most efficient process among those evaluated. The kinetic data thus highlight the strong potential of $LaFeO_3$-based photoelectrocatalysis for the treatment of effluents containing industrial dyes and, by extension, other recalcitrant organic pollutants.

HPLC analysis of R2G

Because photoelectrocatalysis at 15 mA cm^{-2} showed the highest degradation performance, this condition was selected for additional HPLC analysis. Figure 9 presents the chromatographic profiles of Turquoise Tiafix R2G before and after photoelectrocatalytic treatment at different reaction times.

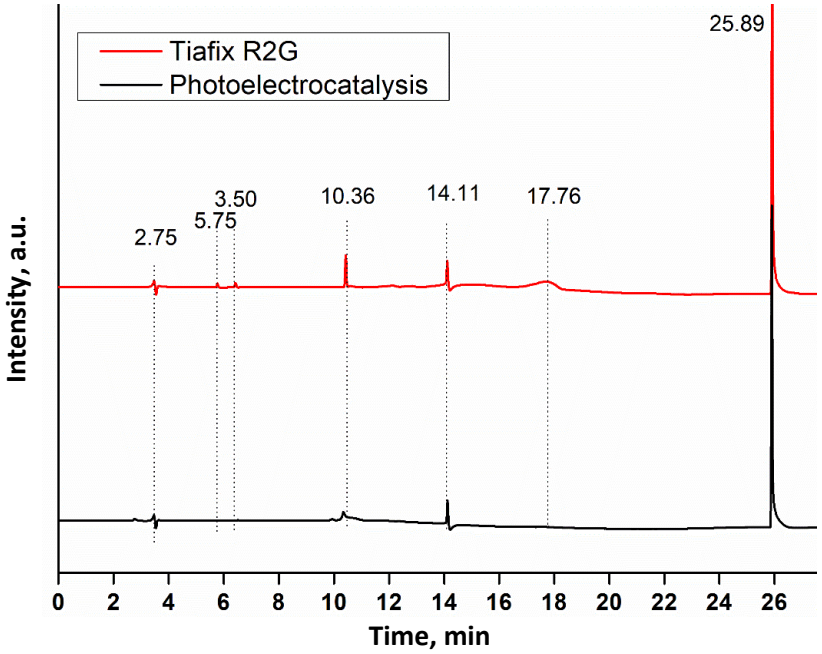

***Figure 9.** HPLC chromatograms of Turquoise Tiafix R2G before and after photoelectrocatalytic treatment, showing the reduction of the main peak and formation of intermediates*

The initial chromatogram exhibits a predominant peak at 25.89 min, attributed to the main dye-related component in the commercial formulation, along with minor peaks that may be associated with impurities, additives, or structurally related species present in the commercial dye formulation. After the photoelectrocatalytic treatment, the area and intensity of the main peak decrease substantially, indicating removal/transformation of the main dye-related component from the solution. At the

same time, additional lower-intensity peaks appear or persist at shorter retention times, suggesting the formation of more polar transformation products during oxidation.

These HPLC results demonstrate that the process involves not only decolorization but also extensive chemical transformation of the pollutant, a distinction that cannot be reliably made by UV-Vis monitoring alone, since transformation products may exhibit similar absorption features. The formation of intermediate compounds is compatible with degradation pathways reported for $LaFeO_3$-based perovskite systems, in which reactive oxygen species, including hydroxyl radicals (•OH) and superoxide radicals ($O_2^{\bullet -}$), participate in the oxidation of aromatic dye structures [17].

Stability and reusability of catalyst

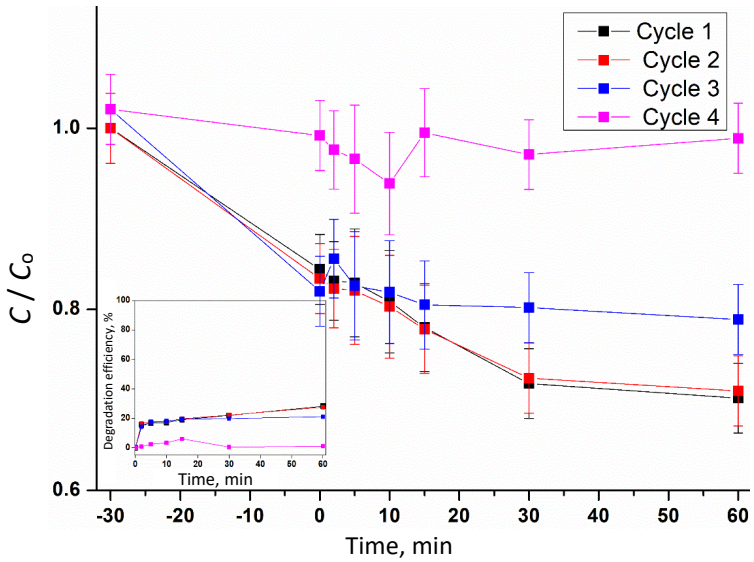

Figure 10. *Reusability of the catalyst under photocatalytic conditions for the degradation of Turquoise Tiafix R2G (200 ppm), over four consecutive cycles*

During the first two cycles, the catalyst displayed comparable degradation efficiencies (29.8 and 29.0 %), indicating short-term stability and effective preservation of surface-active sites under the applied conditions. Similar or even higher stability over several cycles has been reported for mesoporous or supported $LaFeO_3$ systems, which often retain >90 % of their initial activity after 3 to 6 runs [52].

From the third cycle onward, a marked decline in activity was observed (≈21.1%), followed by a drastic loss in the fourth cycle (≈6.1 %), revealing progressive catalyst deactivation under repeated operation. Such behaviour contrasts with $LaFeO_3$ catalysts engineered with hierarchical or porous architectures, which generally exhibit enhanced resistance to deactivation owing to higher surface area and improved mass-transfer pathways.

The loss of activity may be attributed to several factors, including partial catalyst loss during recovery, surface fouling by adsorbed intermediates or by-products, particle agglomeration, and possible changes in the catalyst surface after repeated irradiation and washing steps. These effects can reduce the number of accessible active sites and limit contact between the dye molecules and the photocatalyst surface [23].

Therefore, although the catalyst exhibited acceptable short-term stability during the initial cycles, its reusability under prolonged operation was limited under the conditions tested. These results indicate that future optimization should focus on improving catalyst recovery, surface stability and resistance to fouling.

Conclusions

The synthesized lanthanum ferrite ($LaFeO_3$) presented a well-defined perovskite structure, as confirmed by XRD, while SEM and N_2 adsorption (BET, BJH, DFT) analyses revealed a highly crystalline, densely agglomerated material with low specific surface area and limited porosity. These structural, morphological and textural features support its use in the degradation of the reactive dye Turquoise Tiafix R2G and enabled an integrated assessment of photocatalytic, heterogeneous electro-oxidation and photoelectrocatalytic processes.

Photolysis experiments confirmed the high photostability of R2G under the irradiation conditions employed, with negligible degradation in the absence of catalyst or applied current. In photocatalysis, a $LaFeO_3$ loading of 0.3 g L^{-1} was the most effective among the concentrations tested; however, the process still led to only moderate dye removal, consistent with limitations imposed by electron-hole recombination and the low surface area of the catalyst. Under heterogeneous electro-oxidation at 15 mA·cm^{-2}, dye degradation increased significantly, highlighting the role of the applied current in driving oxidizing species formation, promoting the Fe^{3+}/Fe^{2+} redox cycle in $LaFeO_3$, and intensifying reactions at the electrode-solution interface.

The photoelectrocatalytic process, combining 0.3 g L^{-1} $LaFeO_3$ with a current density of 15 mA cm^{-2} under irradiation, exhibited the best overall performance, reaching near-complete degradation and yielding the highest apparent pseudo-first-order rate constant. Photoelectrocatalysis followed pseudo-first-order kinetics, with an apparent rate approximately 18 times higher than that of photocatalysis and about 5 times higher than that of heterogeneous electro-oxidation, quantitatively demonstrating the synergistic effect between light-driven photocatalytic reactions in suspension and electrochemical oxidant generation at the anode.

HPLC analysis further confirmed the effectiveness of the process by showing a substantial reduction of the main chromatographic peak associated with the parent dye after treatment, along with the formation of intermediate compounds at shorter retention times. These results demonstrate that the observed removal is not limited to decolorization but involves significant chemical transformation of the pollutant, providing more reliable evidence of degradation than UV-Vis analysis alone.

Our results demonstrate that $LaFeO_3$ is a promising material for advanced oxidative processes, with particularly high efficiency under photoelectrocatalytic conditions. The simultaneous application of light and electric current proved to be the most effective strategy, achieving degradation rates substantially higher than those of the isolated photocatalytic and electrochemical processes. Thus, the optimized photoelectrocatalytic system (0.3 g L^{-1} $LaFeO_3$ and 15 mA cm^{-2}) shows considerable potential for application in the treatment of effluents containing industrial dyes and other recalcitrant organic contaminants.

Stability tests showed that the catalyst maintained similar photocatalytic performance during the first two cycles but underwent a progressive decrease in activity after further reuse. This deactivation may be related to partial material loss during recovery, surface fouling by reaction intermediates, or by-products, particle agglomeration and possible surface changes during operation. Therefore, although the catalyst showed acceptable short-term stability, future studies should focus on improving catalyst durability and recovery to enhance its practical applicability in wastewater treatment.

Funding: *This study was financed by CAPES (grant 88887.807550/2023-00), CNPq (grants 305287/2022-2 and 307866/2022-0) and FAPITEC/SE.*

Artificial intelligence statement: *Artificial intelligence tools were used only for language improvement and grammar revision during manuscript preparation. All scientific content, data interpretation, results and conclusions were developed and verified by the authors.*

References

[1] M. Tripathi, S. Singh, S. Pathak, J. Kasaudhan, A. Mishra, S. Bala, D. Garg, R. Singh, P. Singh, P. K. Singh, A. K. Shukla, N. Pathak, Recent Strategies for the Remediation of Textile Dyes from Wastewater, *Toxics* **11** (2023) 940. https://doi.org/10.3390/toxics11110940

[2] C. Caicedo-Montoya, L. S. Copete-Pertuz, G. A. Correa-Londoño, A. L. Mora-Martínez, M. Yepes-Pérez, Decolorization of colored wastewaters with Turquoise Blue dye by the Leptosphaerulina sp. native Colombian fungus-Influence of operational parameters, *DYNA (Colombia)* **89** (2022) 121-131. https://doi.org/10.15446/dyna.v89n221.100185

[3] A. Negi, Environmental Impact of Textile Materials: Challenges in Fiber-Dye Chemistry and Implication of Microbial Biodegradation, *Polymers* **17** (2025) 871. https://doi.org/10.3390/polym17070871

[4] A. A. Alothman, N. Ahmad, M. D. Albaqami, Z. A. ALOthman, K. N. Alqahtani, M. Rizwan Khan, V. Vasanthakumar, Bismuth-doped lanthanum ferrite perovskites: A promising approach for enhancing photo-Fenton degradation of organic dye pollutants, *Ceramics International* **50** (2024) 15867-15878. https://doi.org/10.1016/j.ceramint.2024.02.066

[5] S. Gouadria, A. G. Al-Sehemi, S. Manzoor, M. Abdullah, A. Ghafoor Abid, N. Raza, L. V. Panina, M. I. Sayyed, D. I. Tishkevich, A. V. Trukhanov, Design and preparation of novel $LaFeO_3/NiFe_2O_4$ nanohybrid for highly efficient photodegradation of methylene blue dye under visible light illumination, *Journal of Photochemistry and Photobiology A* **448** (2024) 115305. https://doi.org/10.1016/j.jphotochem.2023.115305

[6] B.M. Pirzada, Pushpendra, R.K. Kunchala, B.S. Naidu, Synthesis of $LaFeO_3/Ag_2CO_3$ Nano-composites for Photocatalytic Degradation of Rhodamine B and p-Chlorophenol under Natural Sunlight, *ACS Omega* **4** (2019) 2618-2629. https://doi.org/10.1021/acsomega.8b02829

[7] O. V. Nkwachukwu, C. Muzenda, B. O. Ojo, B. N. Zwane, B. A. Koiki, B. O. Orimolade, D. Nkosi, N. Mabuba, O. A. Arotiba, Photoelectrochemical degradation of organic pollutants on a La^{3+} doped $BiFeO_3$ perovskite, *Catalysts* **11** (2021) 1069. https://doi.org/10.3390/catal11091069

[8] M. Rodríguez-Peña, R. Natividad, C. E. Barrera-Díaz, P. Balderas Hernández, C. I. Alanis Ramírez, G. Roa-Morales, Current perspective of advanced electrochemical oxidation processes in wastewater treatment and life cycle analysis, *International Journal of Electrochemical Science* **19** (2024) 100589. https://doi.org/10.1016/j.ijoes.2024.100589

[9] A. Mengistu, M. Abewaa, E. Adino, E. Gizachew, J. Abdu, The application of *Rumex abyssinicus* based activated carbon for Brilliant Blue Reactive dye adsorption from aqueous solution, *BMC Chemistry* **17** (2023) 82. https://doi.org/10.1186/s13065-023-01004-2

[10] S. Zhang, X. Lu, X. Liu, K. Fang, J. Gong, J. Si, W. Gao, D. Liu, In Situ Generated UiO-66/Cotton Fabric Easily Recyclable for Reactive Dye Adsorption, *Langmuir* **38** (2022) 12095-12102. https://doi.org/10.1021/acs.langmuir.2c01967

[11] J. Mora-Gómez, M. García-Gabaldón, J. Carrillo-Abad, M.T. Montañés, S. Mestre, V. Pérez-Herranz, Influence of the reactor configuration and the supporting electrolyte concentration on the electrochemical oxidation of Atenolol using BDD and SnO_2 ceramic electrodes, *Separation and Purification Technology* **241** (2020) 116684. https://doi.org/10.1016/j.seppur.2020.116684

[12] D. Song, B. Qiao, X. Wang, L. Zhao, X. Li, P. Zhang, Y. Yao, H. Chen, L. Zhu, H. Sun, Degradation of Perfluorooctanoic Acid by Chlorine Radical Triggered Electrochemical Oxidation System, *Environmental Science and Technology* **57** (2023) 9416-9425. https://doi.org/10.1021/acs.est.3c02025

[13] T. Virtanen, G. Rudolph, A. Lopatina, B. Al-Rudainy, H. Schagerlöf, L. Puro, M. Kallioinen, F. Lipnizki, Analysis of membrane fouling by Brunauer-Emmet-Teller nitrogen adsorption/desorption technique, *Scientific Reports* **10** (2020) 3427. https://doi.org/10.1038/s41598-020-59994-1

[14] E. Allanas, A. Rahman, E. Arlin, E.A. Prasetyanto, *Study surface area and pore size distribution on synthetic zeolite X using BET, BJH and DFT methods*, *Journal of Physics: Conference Series* **2019** (2021) 012094. https://doi.org/10.1088/1742-6596/2019/1/012094

[15] R. S. de S. Castro, A. R. Dória, F. Costa, S. Mattedi, K. I. B. Eguiluz, G. R. Salazar-Banda, Dipropyl ammonium ionic liquids to prepare Ti/RuO_2-Sb_2O_4 anodes at different calcination temperatures, *Environmental Science and Pollution Research* **32** (2025) 10505-10518. https://doi.org/10.1007/s11356-023-29742-9

[16] R. V. Lakshmi, P. Bera, M. Hiremath, V. Dubey, A. K. Kundu, H. C. Barshilia, Structural, magnetic, and dielectric properties of solution combustion synthesized $LaFeO_3$, $LaFe_{0.9}Mn_{0.1}O_3$, and $LaMnO_3$ perovskites, *Physical Chemistry Chemical Physics* **24** (2022) 5462-5478. https://doi.org/10.1039/d1cp05501a

[17] M. Ismael, M. Wark, Perovskite-type $LaFeO_3$: Photoelectrochemical properties and photocatalytic degradation of organic pollutants under visible light irradiation, *Catalysts* **9** (2019) 342. https://doi.org/10.3390/catal9040342

[18] O. Wiranwetchayan, S. Promnopas, S. Phadungdhitidhada, A. Phuruangrat, T. Thongtem, P. Singjai, S. Thongtem, Characterization of perovskite $LaFeO_3$ synthesized by microwave plasma method for photocatalytic applications, *Ceramics International* **45** (2019) 4802-4809. https://doi.org/10.1016/j.ceramint.2018.11.175

[19] Y. Ye, H. Yang, X. Wang, W. Feng, Photocatalytic, Fenton and photo-Fenton degradation of RhB over Z-scheme g-C_3N_4/$LaFeO_3$ heterojunction photocatalysts, *Materials Science in Semiconductor Processing* **82** (2018) 14-24. https://doi.org/10.1016/j.mssp.2018.03.033

[20] B. Kucharczyk, J. Okal, W. Tylus, J. Winiarski, B. Szczygieł, The effect of the calcination temperature of $LaFeO_3$ precursors on the properties and catalytic activity of perovskite in methane oxidation, *Ceramics International* **45** (2019) 2779-2788. https://doi.org/10.1016/j.ceramint.2018.07.299

[21] A. Hameed, A. Asghar, S. Shabbir, I. Ahmed, A.K. Tareen, K. Khan, G. Hussain, M. Y. Awaji, H. Anwar, A detailed investigation of rare earth lanthanum substitution effects on the structural, morphological, vibrational, optical, dielectric and magnetic properties of Co-Zn spinel ferrites, *Frontiers in Chemistry* **12** (2024) 1433004. https://doi.org/10.3389/fchem.2024.1433004

[22] D. Navas, S. Fuentes, A. Castro-Alvarez, E. Chavez-Angel, Review on Sol-Gel Synthesis of Perovskite and Oxide Nanomaterials, *Gels* **7** (2021) 275. https://doi.org/10.3390/gels7040275

[23] T. T. N. Phan, A. N. Nikoloski, P. A. Bahri, D. Li, Adsorption and photo-Fenton catalytic degradation of organic dyes over crystalline $LaFeO_3$-doped porous silica, *RSC Advances* **8** (2018) 36181-36190. https://doi.org/10.1039/c8ra07073c

[24] Y. Li, X. Meng, Y. Pang, C. Zhao, D. Peng, Y. Wei, B. Xiang, Activation of bisulfite by $LaFeO_3$ loaded on red mud for degradation of organic dye, *Royal Society Open Science* **9** (2022) 220466. https://doi.org/10.1098/rsos.220466

[25] W. Sun, H. Wei, L. yang An, C. Jin, H. Wu, Z. ang Xiong, C. Pu, C. Sun, Oxygen vacancy mediated $La_{1-x}Ce_xFeO_{3-\delta}$ perovskite oxides as efficient catalysts for CWAO of acrylic acid by A-site Ce doping, *Applied Catalysis B* **245** (2019) 20-28. https://doi.org/10.1016/j.apcatb.2018.12.024

[26] C. Cheng, S. Gao, J. Zhu, G. Wang, L. Wang, X. Xia, Enhanced performance of $LaFeO_3$ perovskite for peroxymonosulfate activation through strontium doping towards 2,4-D degradation, *Chemical Engineering Journal* **384** (2020) 123377. https://doi.org/10.1016/j.cej.2019.123377

[27] C. Lara-Pérez, E. Leyva, B. Zermeño, I. Osorio, C. Montalvo, E. Moctezuma, Photocatalytic degradation of diclofenac sodium salt: adsorption and reaction kinetic studies, *Environmental Earth Sciences* **79** (2020) 277. https://doi.org/10.1007/s12665-020-09017-z

[28] I. Khan, K. Saeed, I. Zekker, B. Zhang, A.H. Hendi, A. Ahmad, S. Ahmad, N. Zada, H. Ahmad, L.A. Shah, T. Shah, I. Khan, Review on Methylene Blue: Its Properties, Uses, Toxicity and Photodegradation, *Water* **14** (2022) 242. https://doi.org/10.3390/w14020242

[29] Y.H. Chiu, T.F.M. Chang, C.Y. Chen, M. Sone, Y.J. Hsu, Mechanistic insights into photodegradation of organic dyes using heterostructure photocatalysts, *Catalysts* **9** (2019) 430. https://doi.org/10.3390/catal9050430

[30] N.K. Gupta, Y. Ghaffari, S. Kim, J. Bae, K.S. Kim, M. Saifuddin, Photocatalytic Degradation of Organic Pollutants over MFe_2O_4 (M = Co, Ni, Cu, Zn) Nanoparticles at Neutral pH, *Scientific Reports* **10** (2020) 4942. https://doi.org/10.1038/s41598-020-61930-2

[31] A. I. Alwared, N. A. Mohammed, T. J. Al-Musawi, A. A. Mohammed, Solar-Induced Photocatalytic Degradation of Reactive Red and Turquoise Dyes Using a Titanium Oxide/Xanthan Gum Composite, *Sustainability* **15** (2023) 10815. https://doi.org/10.3390/su151410815

[32] A. A. Ansari, S. F. Adil, M. Alam, N. Ahmad, M. E. Assal, J. P. Labis, A. Alwarthan, Catalytic performance of the Ce-doped $LaCoO_3$ perovskite nanoparticles, *Scientific Reports* **10** (2020) 15012. https://doi.org/10.1038/s41598-020-71869-z

[33] H. Awang, A. Hezam, T. Peppel, J. Strunk, Enhancing the Photocatalytic Activity of Halide Perovskite Cesium Bismuth Bromide/Hydrogen Titanate Heterostructures for Benzyl Alcohol Oxidation, *Nanomaterials* **14** (2024) 752. https://doi.org/10.3390/nano14090752

[34] W. Zhang, Y. Ma, X. Zhu, S. Liu, T. An, J. Bao, X. Hu, H. Tian, Fabrication of Ag decorated g-C_3N_4/$LaFeO_3$ Z-scheme heterojunction as highly efficient visible-light photocatalyst for degradation of methylene blue and tetracycline hydrochloride, *Journal of Alloys and Compounds* **864** (2021) 158914. https://doi.org/10.1016/j.jallcom.2021.158914

[35] O. V. Nkwachukwu, O. A. Arotiba, Perovskite Oxide-Based Materials for Photocatalytic and Photoelectrocatalytic Treatment of Water, *Frontiers in Chemistry* **9** (2021) 634630. https://doi.org/10.3389/fchem.2021.634630

[36] Y. L. Lee, M. J. Gadre, Y. Shao-Horn, D. Morgan, *Ab initio* GGA+U study of oxygen evolution and oxygen reduction electrocatalysis on the (001) surfaces of lanthanum transition metal perovskites $LaBO_3$ (B = Cr, Mn, Fe, Co and Ni), *Physical Chemistry Chemical Physics* **17** (2015) 21643-21663. https://doi.org/10.1039/c5cp02834e

[37] S. Cotillas, J. Llanos, P. Cañizares, D. Clematis, G. Cerisola, M. A. Rodrigo, M. Panizza, Removal of Procion Red MX-5B dye from wastewater by conductive-diamond electrochemical oxidation, *Electrochimica Acta* **263** (2018) 1-7. https://doi.org/10.1016/j.electacta.2018.01.052

[38] F. L. Souza, C. Sáez, P. Cañizares, M. A. Rodrigo, Improving photolytic treatments with electrochemical technology, *Separation and Purification Technology* **235** (2020) 116229. https://doi.org/10.1016/j.seppur.2019.116229

[39] P. Fernandez-Ibanez, S. McMichael, A. Rioja Cabanillas, S. Alkharabsheh, A. Tolosana Moranchel, J.A. Byrne, New trends on photoelectrocatalysis (PEC): nanomaterials, wastewater treatment and hydrogen generation, *Current Opinion in Chemical Engineering* **34** (2021) 100725. https://doi.org/10.1016/j.coche.2021.100725

[40] T. X. Nguyen, Y. C. Liao, C. C. Lin, Y. H. Su, J. M. Ting, Advanced High Entropy Perovskite Oxide Electrocatalyst for Oxygen Evolution Reaction, *Advanced Functional Materials* **31** (2021) 2101632. https://doi.org/10.1002/adfm.202101632

[41] J. O. Bockris, T. Otagawa, The Electrocatalysis of Oxygen Evolution on Perovskites, *Journal of The Electrochemical Society* **131** (1984) 290-302. https://doi.org/10.1149/1.2115565

[42] W. Dong, W. Qiao, S. Xiong, J. Yang, X. Wang, L. Ding, Y. Yao, Q. Bao, Surface Passivation and Energetic Modification Suppress Nonradiative Recombination in Perovskite Solar Cells, *Nano-Micro Letters* **14** (2022) 108. https://doi.org/10.1007/s40820-022-00854-0

[43] M. Pavel, C. Anastasescu, R. N. State, A. Vasile, F. Papa, I. Balint, Photocatalytic Degradation of Organic and Inorganic Pollutants to Harmless End Products: Assessment of Practical Application Potential for Water and Air Cleaning, *Catalysts* **13** (2023) 380. https://doi.org/10.3390/catal13020380

[44] A. Al Miad, S. P. Saikat, M. K. Alam, M. Sahadat Hossain, N. M. Bahadur, S. Ahmed, Metal oxide-based photocatalysts for the efficient degradation of organic pollutants for a sustainable environment: a review, *Nanoscale Advances* **6** (2024) 4781-4803. https://doi.org/10.1039/d4na00517a

[45] B. A. Marinho, L. Suhadolnik, B. Likozar, M. Huš, Ž. Marinko, M. Čeh, Photocatalytic, electrocatalytic and photoelectrocatalytic degradation of pharmaceuticals in aqueous media: Analytical methods, mechanisms, simulations, catalysts and reactors, *Journal of Cleaner Production* **343** (2022) 131061. https://doi.org/10.1016/j.jclepro.2022.131061

[46] X. Song, P. Yuan, X. Xu, J. Yang, Mechanism and Performance of Electrocatalytic Oxidation on RuO_2-IrO_2@Ti Anode in Alkaline Phenol Wastewater, *ACS Omega* **10** (2025) 34471-34484. https://doi.org/10.1021/acsomega.5c02679

[47] A.T. Tomaz, C.R. Costa, M. de Lourdes S. Vasconcellos, R. Pedicini, J. Ribeiro, Evaluation of Photoelectrocatalysis with Electrode Based on Ti/RuO_2-TiO_2 Modified with Tin and Tantalum Oxides for the Degradation of Indigo Blue Dye, *Nanomaterials* **12** (2022) 4301. https://doi.org/10.3390/nano12234301

[48] M. O. Santos, G. de O. S. Santos, S. Mattedi, S. Griza, K.I. Katlin, G.R. Salazar-Banda, Influence of the calcination temperature and ionic liquid used during synthesis procedure on the physical and electrochemical properties of Ti/$(RuO_2)_{0.8}$-$(Sb_2O_4)_{0.2}$ anodes, *Journal of Electroanalytical Chemistry* **829** (2018) 116-128. https://doi.org/10.1016/j.jelechem.2018.10.013

[49] J. Katiyar, V. K. Saharan, Enhanced photocatalytic degradation of reactive blue 21 dye and textile dyeing effluent by synthesized $SmFeO_3$-rGO photocatalyst in combination with ultrasonication: Characterization and performance evaluation, *Journal of Water Process Engineering* **56** (2023) 104314. https://doi.org/10.1016/j.jwpe.2023.104314

[50] K. M. S. Khalil, A.H. Mahmoud, M. Khairy, Formation and textural characterization of size-controlled $LaFeO_3$ perovskite nanoparticles for efficient photocatalytic degradation of organic pollutants, *Advanced Powder Technology* **33** (2022) 103429. https://doi.org/10.1016/j.apt.2022.103429

[51] L. Zou, C. Tian, Z. Lin, Y. Wang, T. Gu, Z. Wang, T. Tang, H. Shi, Enhanced photocatalytic degradation of organic dyes by La^{3+} doped $SrBi_4Ti_4O_{15}$, *Ceramics International* **50** (2024) 45369-45381. https://doi.org/10.1016/j.ceramint.2024.08.377

[52] T. T. N. Phan, H. L. Nguyen, V. T. Le, C. N. Phan, T. H. Pham, Mesoporous $LaFeO_3$: Synergistic Effect of Adsorption and Visible Light Photo-Fenton Processes for Phenol Removal from Refinery Wastewater, *Journal of Chemistry* (2021) 5841066. https://doi.org/10.1155/2021/5841066